

DOI: 10.1002/cphc.201300568

# A Potential Carcinogenic Pyrene Derivative under Förster Resonance Energy Transfer to Various Energy Acceptors in Nanoscopic Environments

Soma Banerjee, Nirmal Goswami, and Samir Kumar Pal<sup>\*[a]</sup>

Picosecond-resolved Förster resonance energy transfer (FRET) from various vibronic bands in benzo[*a*]pyrene (BP) shows a strong dependency on the spectral overlap of an energy acceptor in a confined environment. Our study on the dipolar interactions between BP and different acceptors, including ethidium (Et), acridine orange (AO), and crystal violet (CV), at the surface of a model anionic micelle revealed that the Förster distance ( $R_0$ ) and the rate of energy transfer is dependent on the individual spectral overlap of the vibronic bands of BP with the absorption spectra of the different energy acceptors. The differential behavior of the vibronic bands is compared with

that of different dyes [quantum dots (QDs)] in a “dye-blend” (mixture) under FRET to an energy acceptor. Comparison of the FRET of the QDs with that of BP confirmed the independent nature of the dipolar interaction of the vibronic bands with other organic molecules, and the use of deconvolution techniques in the interpretation of the donor–acceptor (D–A) distance was also justified. We also showed that the consideration of differential FRET from the vibronic bands of BP and from the QDs in the dye-blend is equally acceptable in theoretical frameworks including the Infelta–Tachiya model and D–A distribution analysis in nanoenvironments.

## 1. Introduction

Pyrenes belong to the polycyclic aromatic hydrocarbons (PAHs) class of compounds and have several appealing photophysical properties that make them suitable for use as effective fluorescence probes.<sup>[1–4]</sup> One of those properties is the sensitivity of their spectral parameters, such as changes in their vibronic structures (especially the intensity ratios of the first and third vibronic bands) as a result of changes in the environment.<sup>[5]</sup> The effects of temperature and solute–solvent interactions on the various vibronic fine structures in the emission spectra of the pyrene class of compounds have been well explored,<sup>[2,6,7]</sup> and these studies revealed the differential perturbation of the individual vibronic bands. Benzo[*a*]pyrene (BP), a well-known pyrene derivative and a potential carcinogen to which humans are most frequently exposed,<sup>[8]</sup> exhibits differential shifts of its individual vibronic structures as a function of the refractive index of the surrounding solvent.<sup>[6]</sup> BP is a byproduct of grilled foods,<sup>[9]</sup> tobacco,<sup>[10]</sup> and fuel combustion and has long been linked to various human cancers, particularly lung and skin cancers. Though there have been extensive studies on environmental effects on the steady-state fluorescence spectrum of pyrene,<sup>[2]</sup> solvatochromism of BP as manifested through shifts in its excitation and emission bands in a wide variety of solvents,<sup>[6]</sup> the effects of different solvents on the excited-state

lifetime at different vibronic bands of such molecules, and highlighting the consequences of solvent dipole/dielectric constant on nonradiative rates have been much less explored.

Another important aspect is the dipolar interaction of the pyrene class of dyes with other molecules manifested in Förster resonance energy transfer (FRET). The differential behavior of the individual vibronic bands in the emission spectra of pyrene and its derivatives in response to changes in temperature,<sup>[7]</sup> polarity,<sup>[2]</sup> and refractive index<sup>[6]</sup> of the host solvent is well known, whereas reports on the behavior of these bands while undergoing dipolar interactions with different molecules are still lacking. FRET, which is also known as a “spectroscopic ruler”,<sup>[11–13]</sup> is very often used to measure the distance between two sites on a macromolecule.<sup>[14]</sup> As pyrene and its derivatives are known to interact with biological macromolecules,<sup>[6,15]</sup> FRET can serve as an efficient tool to investigate the biomolecular recognition of these molecules. In an earlier study,<sup>[16]</sup> attempts to use FRET from pyrenes to perylene were made for nucleic acid assays under homogeneous solution conditions by using steady-state spectroscopy. In another recent study,<sup>[17]</sup> FRET was used as a tool to detect the antibody binding of PAHs by using a hydroxyl derivative of BP as a FRET donor and sulforhodamine B as the energy acceptor by employing both steady-state and time-resolved spectroscopy. However, investigation of the vibronic bands under dipolar coupling was beyond the scope of those studies. Notably, estimation of the donor–acceptor (D–A) distance from steady-state FRET studies was found to be inconclusive.<sup>[18]</sup>

Here, we studied the excited-state fluorescence relaxation dynamics of BP in a number of solvents with various dipole moments/refractive indices. We compared the relaxation dy-

[a] S. Banerjee, N. Goswami, Dr. S. K. Pal  
Department of Chemical, Biological & Macromolecular Sciences  
S. N. Bose National Centre for Basic Sciences  
Block JD, Sector III, Salt Lake  
Kolkata 700 098 (India)  
E-mail: skpal@bose.res.in

 Supporting information for this article is available on the WWW under <http://dx.doi.org/10.1002/cphc.201300568>.

namics of the vibronic bands in the solvents to investigate the effects of solvent polarity and dipole moment on the excited-state lifetime of BP at various emission wavelengths. Steady-state and time-resolved experiments of BP in the anionic micellar solutions confirmed the location of the probe BP. To study the dipolar interaction of BP with another organic dye, we monitored FRET from BP to a well-characterized acceptor (and potential mutagen),<sup>[19]</sup> ethidium (Et), which selectively binds to the surface of the micelle.<sup>[20,21]</sup> Steady-state and picosecond-resolved studies on the FRET between BP and Et from various vibronic bands were analyzed by using conventional and differential methods. The differential method introduced in this study relies on the individual spectral overlap of the vibronic bands with the absorption spectrum of the Et acceptor and was found to be more realistic for the estimation of the D–A distance. We also studied FRET between BP and acridine orange (AO) in the micelle to establish generality of the technique for the estimation of the D–A distance. Unambiguous confirmation of the introduced technique was revealed from the FRET from BP to crystal violet<sup>[22]</sup> (CV) in the nanoenvironments. CV was observed to offer significant and negligibly small spectral overlap with band 3 (emission peak at 455 nm) and band 1 (emission peak at 410 nm), respectively. The differential behavior of the vibronic bands of BP undergoing dipolar interaction with energy acceptors in the micellar solution was compared with that of different dyes in a model system of “dye-blend” (mixture of dyes) representing different electronic systems undergoing FRET with CV in toluene. In this regard, three different quantum dots (QDs), QD480, QD570, and QD625 having emission maxima at 480, 570, and 625 nm, respectively, were considered as the components of the dye-blend. A theoretical framework employing the well-known Infelta–Tachiya model<sup>[21]</sup> and D–A distance distribution analysis were also considered in our study to further establish the validity of the introduced differential technique of FRET calculation.

## 2. Results and Discussion

### Effects of Different Solvents on the Excited-State Lifetime of BP

The normalized absorption and emission spectra of BP in various solvents are presented in Figure 1a. Solvent-dependent shifting of both the absorption and fluorescence spectra of BP is in close agreement with earlier studies,<sup>[6]</sup> and this shifting is suggestive of solvent-sensitive changes in the ground-state and excited-state electronic properties of BP. The picosecond-resolved fluorescence transients of BP in different solvents are shown in Figure 1b with an emission wavelength ( $\lambda_{em}$ ) of 410 nm and an excitation wavelength ( $\lambda_{ex}$ ) of 375 nm, and the multiexponential fitting parameters are tabulated in Table 1. Figure 1b and Table 1 indicate that the lifetime of BP varies with solvents without much deviation at the different vibronic fine structures. As is evident from Table 1, BP shows biexponential decay with time constants of 2–5 and 12–20 ns in all of the solvents. Notably, the absorption and emission spectra of

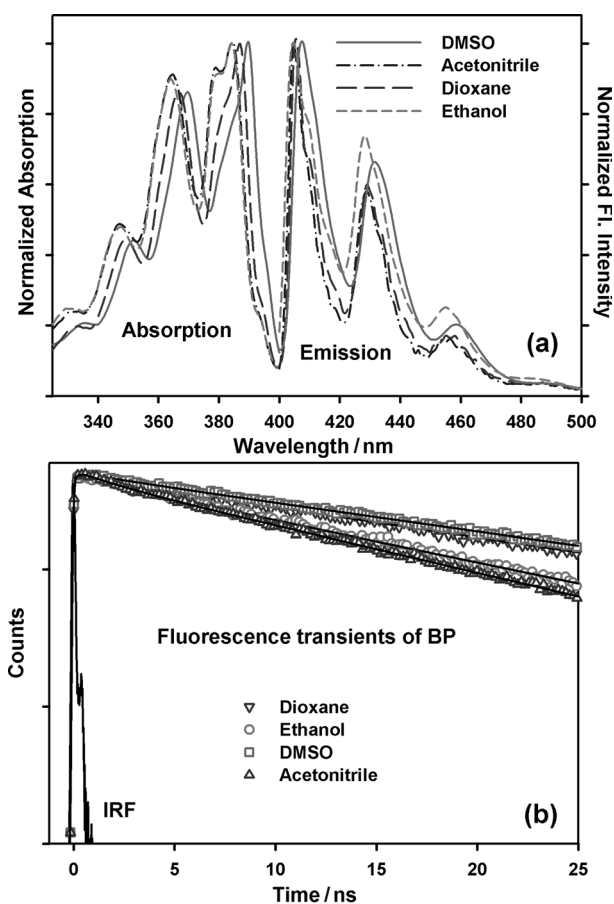


**Figure 1.** a) Normalized absorption and emission spectra of BP in DMSO, acetonitrile, dioxane, and ethanol; b) fluorescence transients of BP in DMSO, acetonitrile, dioxane, and ethanol;  $\lambda_{em} = 410$  nm,  $\lambda_{ex} = 375$  nm.

**Table 1.** Lifetime components ( $\tau$ ) of BP at its characteristic emission peaks in various solvents.

Sample	$\lambda_{em}$ [nm]	$\tau_1$ [ns]	$\tau_2$ [ns]	$\tau_{av}^{(b)}$ [ns]
BP in DMSO	410	2.00 (5)	20.10 (95)	19.20
	430	2.00 (10)	20.10 (90)	18.30
	455	2.00 (20)	20.50 (80)	16.80
BP in acetonitrile	410	2.10 (12)	12.50 (88)	11.30
	430	1.80 (14)	12.60 (86)	11.10
	455	1.60 (26)	12.60 (74)	9.70
BP in dioxane	410	5.00 (9)	20.30 (91)	18.90
	430	5.00 (11)	20.40 (89)	18.70
	455	5.00 (20)	20.70 (80)	17.60
BP in ethanol	410	3.60 (10)	14.20 (90)	13.20
	430	3.30 (11)	14.20 (89)	13.00
	455	3.30 (20)	14.00 (80)	11.90

[a] Relative contribution of the component. [b]  $\tau_{av}$  is the average lifetime. Error  $\pm 5\%$ .

BP in all of the solvents are consistent with those of the monomeric form of BP.<sup>[6]</sup> No clear correlation of the excited-state lifetime with the polarity/proticity of the solvents is evident from Table 1. For example, the lifetime of BP in DMSO (polar, aprotic) and dioxane (nonpolar, aprotic) is similar. A similar lifetime

in ethanol (polar, protic) and acetonitrile (polar, aprotic) is also noticeable. In an earlier study involving the use of steady-state spectroscopy, it was shown that spectral shifts in the vibronic bands of BP depend on the polarizability (i.e. dielectric constant) of the host solvents.<sup>[6]</sup> We also investigated the polarizability dependence of radiative rate constants of BP in various solvents with different refractive indices. The excited-state lifetimes of BP in various solvents are tabulated in Table S1 (see the Supporting Information). It is evident from Figure S1 that the experimental values of the radiative rate constants ( $k_r$ , shown in dots) of BP in different solvents are significantly different from theoretical estimations (solid line) by following different theoretical models.<sup>[23]</sup> Therefore, a distinct correlation of the spectral shift/lifetime of the vibronic fine structures with the dipole moment/dielectric constant/refractive index is not evident from our studies. Therefore, a more in-depth study is required, and this is motivation for our future work. However, excited-state photophysics, including the fluorescence lifetime of BP in various solvents, is useful to conclude the location of the BP probe in a micro-heterogeneous environment. The extreme hydrophobicity of BP drives it to the lipophilic interior of the sodium dodecyl sulfate (SDS) micelle, as observed previously,<sup>[6,24]</sup> and comparison of the emission spectrum and excited-state lifetime of BP in dioxane (nonpolar, aprotic) with those in the SDS micelle (Figure 2) clearly reveals that the BP

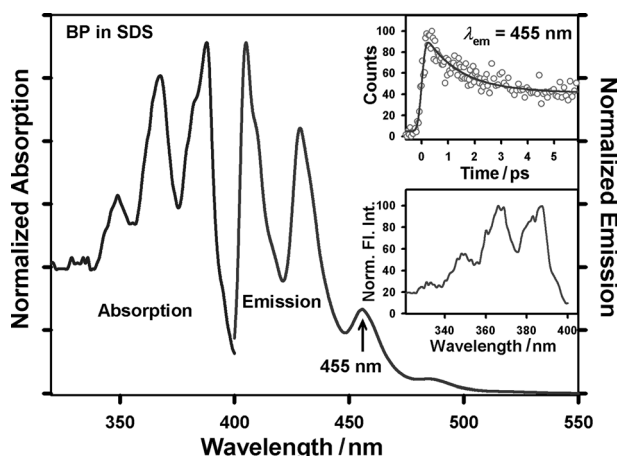


**Figure 2.** Normalized absorption and emission spectra of BP in the SDS micelle. Lower inset shows the normalized excitation spectrum of BP in the SDS micelle. Upper inset shows femtosecond-resolved fluorescence transient of BP;  $\lambda_{em} = 455$  nm,  $\lambda_{ex} = 375$  nm.

probe prefers to stay in the hydrophobic core of the micelle, which is in close agreement with earlier studies.<sup>[6,24]</sup>

### Photophysical Characterization of the Excited BP Molecules

Upon excitation with a laser source of 375 nm, the BP molecules are typically excited to  $S_1$ , usually to an excited vibrational level. Multiple bands in the absorption spectrum of BP in SDS solution at 330, 349, 368, and 388 nm (Figure 2) are assigned to the individual electronic transitions of BP as reported earlier.<sup>[25]</sup> The molecular symmetry of BP<sup>[25]</sup> is  $C_s$ , and this allows

an infinite number of possible moment directions for electric-dipole-allowed transitions: perpendicular to the molecular plane (e.g.  $\sigma \rightarrow \pi^*$ ) or along any direction in this plane ( $\pi \rightarrow \pi^*$ ). The angle,  $\Phi$ , formed by the moments of the observed transitions with a specific, well-defined molecular axis in the plane was reported<sup>[25]</sup> to be  $30^\circ$  for electronic transitions at 330, 349, 368, and 388 nm. The orientation factor,  $K_r$ , the average cosine square of the angle between the moment of transition and the molecular orientation axis, was also reported with a value of 0.56 for the above electronic transitions.<sup>[25]</sup>

An interesting consequence of emission to higher vibrational ground states is that the emission spectrum is typically a mirror image of the absorption spectrum of the  $S_0 \rightarrow S_1$  transition (Figure 2). This similarity occurs because electronic excitation does not greatly alter the nuclear geometry.<sup>[26]</sup> The upper inset in Figure 2 shows the femtosecond-resolved fluorescence transient of BP in the SDS micelle at 455 nm upon excitation of the probe at 375 nm. The transient can be fitted biexponentially with time constants of 1.33 ps (61%) and 30 ns (39%). The slower component of 30 ns was obtained from picosecond-resolved experiments (see below) and was fixed in the above fitting. The faster time constant (1.33 ps) is close to the time constant of about 2 ps, which was assigned to the vibrational cooling of the  $S_1$  local pyrene state that was initially formed with an excess amount of vibrational energy.<sup>[27]</sup> The lower inset of Figure 2 shows the excitation spectrum of BP in the SDS micelle, and it is identical for each vibronic structure; thus, the possibility of the accumulation of different excited states can be ruled out.

### Differential Behavior of the Vibronic Bands of BP under FRET

To monitor the characteristic behavior of the different vibronic bands of BP while undergoing dipolar interactions, we employed FRET studies. For such studies, we used Et as a well-characterized FRET acceptor at the surface of the anionic micelle.<sup>[20,21]</sup> Figure 3a shows the overlap between the emission spectrum of BP (donor) and the absorption spectrum of Et (acceptor) in the SDS micelle. Notably, FRET analysis with consideration of the overall overlap integral,  $J(\lambda)$ , of the BP emission spectrum with the Et absorption spectrum is unable to rationalize the following two observations that are evident from Figure 3. First, different vibronic bands undergo different degrees of fluorescence quenching (Figure 3c). Second, the picosecond-resolved nonradiative energy-transfer rates from various vibronic bands are also significantly different (Figure 3d–f and Table 3). The D–A distance estimated with this analysis process also reveals significant fluctuation in the values reported from different vibronic bands. The above anomaly can easily be addressed if the individual values of  $J(\lambda)$  for each vibronic band in the absorption spectrum of Et are considered. The deconvoluted emission spectra of BP at its three well-characterized emission peaks (410, 430, and 455 nm) are shown in Figure 3b. Notably, the BP monomers also produce a weak emission band at around 480 nm,<sup>[28]</sup> which was not considered in this study. The overlap integral,  $J(\lambda)$ , between the deconvoluted

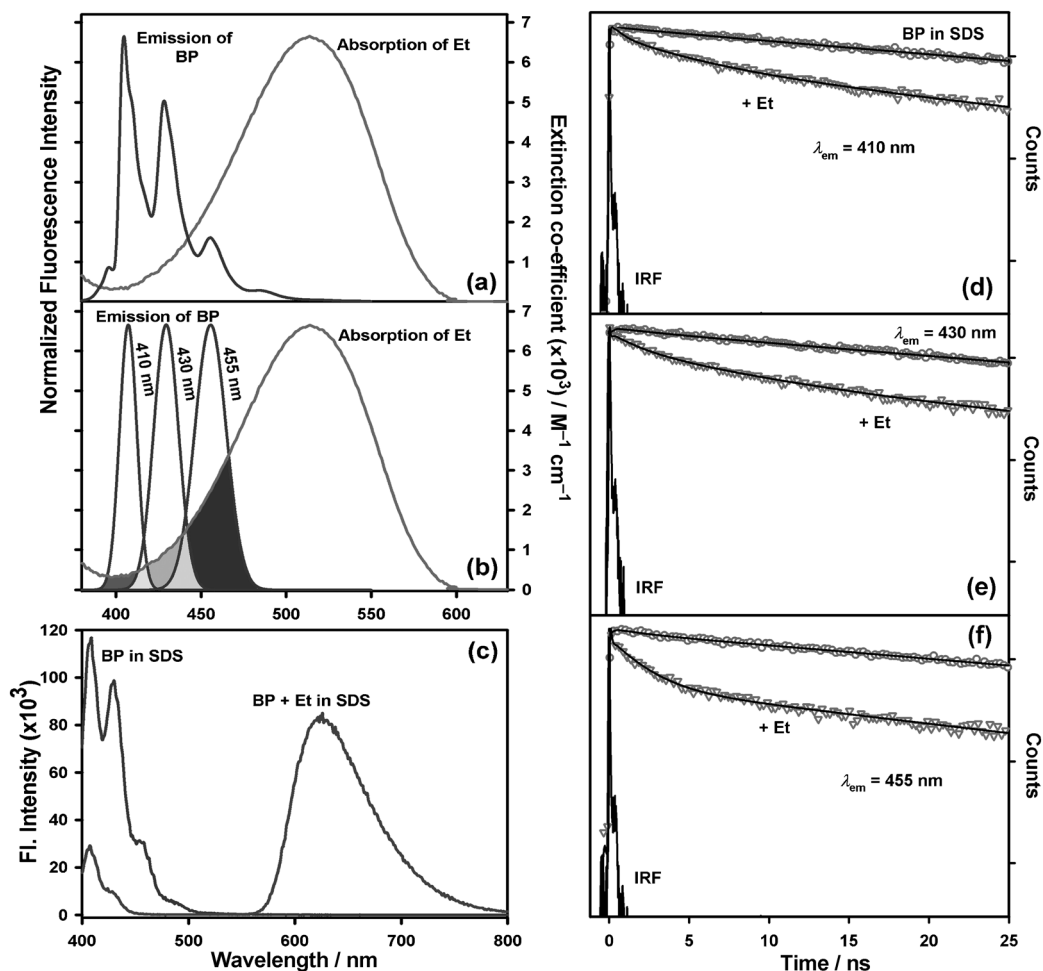


**Figure 3.** Overlap of the emission spectrum of BP with the absorption spectrum of Et in 100 mM SDS ( $\approx 1.48$  mM micellar concentration) without (a) and with (b) the deconvolution of the emission spectrum of BP at specific wavelengths of 410, 430, and 455 nm. c) The emission spectrum of BP in the SDS micelle before and after the addition of the Et acceptor. Picosecond-resolved fluorescence transients of the BP donor molecules bound to SDS micelles with ( $\nabla$ ) and without ( $\circ$ ) the Et acceptor at d) 410, e) 430, and f) 455 nm.  $\lambda_{\text{ex}} = 350$  nm for (a) and (b) and  $\lambda_{\text{ex}} = 375$  nm for (c)–(f).

luted emission spectrum of the donor and the absorption spectrum of the acceptor was characterized for each vibronic band, as shown in Figure 3b. The corresponding values of  $J(\lambda)$  are tabulated in Table 2. The energy transfer takes place from the donor to the acceptor, as indicated by the quenching of the fluorescence intensity (Figure 3c) as well as by the faster decay (Figure 3d–f) of the donor in the D–A complexes in micelles relative to that of only the donor in the micelles. To compare the energy-transfer efficiency of the donor from its vari-

ous vibronic bands, the fluorescence transients of the donor at its different emission peaks (410, 430, and 455 nm) were monitored in the absence and in the presence of the Et acceptor (Figure 3d–f and Table 3).

As evidenced from Figure 3d–f and Table 3, the average lifetime of BP at 410, 430, and 455 nm is 29.92, 29.46, and 27.84 ns respectively. The slower component of 30 ns in the fluorescence transients of BP in the SDS micelle, as given in Table 3, was confirmed by repeating the experiments with a longer time of 400 ns. Details of the FRET parameters from various vibronic bands are tabulated in Table 2. Notably, the vibrational relaxation timescale as observed from our femtosecond-resolved experiments is much faster than the energy-transfer rates from the vibronic bands. Thus, FRET is expected to occur after the thermalization process in the excited state. It is clear that the energy-transfer efficiency ( $E$ ) is higher at 455 nm than at 410 nm, and this is consistent with the overlap integral,  $J(\lambda)$ , between the deconvoluted donor emission at the corresponding wavelengths with the absorption spectrum of the Et acceptor (Figure 3b). From our time-resolved studies, the D–A distance ( $r$ ) can be estimated to be  $(1.95 \pm 0.08)$  nm

**Table 2.** Comparison of the Förster distance ( $R_0$ ), overlap integral  $J(\lambda)$  (between the emission spectrum of the BP donor and the absorption spectrum of the Et acceptor) obtained at the three deconvoluted emission peaks of the donor along with the energy transfer efficiency ( $E$ ) and D–A distance ( $r$ ) calculated from time-resolved experiments in the presence of the Et acceptor.

$\lambda_{\text{em}}(\text{BP})$ [nm]	$R_0$ [nm]	$J(\lambda)$ [ $\text{M}^{-1}\text{cm}^{-1}\text{nm}^4$ ]	$E$ [%]	$r$ [nm]
410	2.16	$1.09 \times 10^{13}$	64	1.96
430	2.59	$3.44 \times 10^{13}$	81	2.03
455	2.47	$1.12 \times 10^{14}$	84	1.87

**Table 3.** Lifetime components ( $\tau$ ) of the BP donor in the SDS micelle in the absence and in the presence of the Et, AO, and CV acceptors.

Sample	$\lambda_{em}$ [nm]	$\tau_1$ [ns] (rel. contrib. [%]) <sup>[a]</sup>	$\tau_2$ [ns] (rel. contrib. [%]) <sup>[a]</sup>	$\tau_3$ [ns] (rel. contrib. [%]) <sup>[a]</sup>	$\tau_{av}$ <sup>[b]</sup> [ns]
BP in SDS micelle	410	4.80 (3)	30.70 (97)	–	29.90
	430	2.90 (5)	30.90 (95)	–	29.50
	455	2.50 (10)	30.70 (90)	–	27.80
BP in SDS micelle + Et	410	0.50 (28)	4.50 (36)	25.40 (36)	10.90
	430	0.10 (59)	4.20 (23)	24.90 (18)	5.50
	455	0.10 (56)	2.30 (30)	27.00 (14)	4.50
BP in SDS micelle + AO	410	0.10 (21)	2.10 (24)	28.20 (55)	16.00
	430	0.10 (63)	2.50 (22)	25.20 (15)	4.40
	455	3.50 (96)	15.50 (4)	–	4.00
BP in SDS micelle + CV	410	4.90 (3)	30.70 (97)	–	29.90
	430	0.10 (81)	1.90 (3)	24.80 (16)	4.10
	455	0.10 (89)	2.20 (1)	24.70 (10)	2.60

[a] Relative contribution of the component. [b]  $\tau_{av}$  is the average lifetime. Error  $\pm 5\%$ .

and the fluctuation (0.8 Å) is well within the experimental error limit.

Upon finding the energy-transfer efficiency of the individual vibronic bands of BP undergoing FRET with the Et acceptor molecules, AO was chosen as another acceptor to find consistency within the results. AO, a cationic dye, is known to interact with the SDS micelle through both hydrophobic and electrostatic interactions, as the hydrophobic aromatic rings of AO remain within the hydrophobic core of the SDS micelle, and the charged intracyclic imino group and the two terminal polar amino groups are directed out towards the stern layer.<sup>[29–31]</sup> Figure 4a,b show the overall and deconvoluted spectral overlap, respectively, between the emission spectrum of BP (donor) and the absorption spectrum of AO (acceptor) in the micelle. The overlap integral,  $J(\lambda)$ , between the deconvoluted emission spectrum of the donor and the absorption spectrum of the AO acceptor was characterized for each emission peak and is tabulated in Table 4. Quenching of the fluores-

**Table 4.** Comparison of the Förster distance ( $R_0$ ), overlap integral  $J(\lambda)$  (between the emission spectrum of the BP donor and the absorption spectrum of the AO acceptor) obtained at the three deconvoluted emission peaks of the donor along with the energy transfer efficiency ( $E$ ) and the D–A distance ( $r$ ) calculated from time-resolved experiments in the presence of the AO acceptor.

$\lambda_{em}$ (BP) [nm]	$R_0$ [nm]	$J(\lambda)$ [ $M^{-1} cm^{-1} nm^4$ ]	$E$ [%]	$r$ [nm]
410	2.68	$3.99 \times 10^{13}$	46	2.75
430	3.08	$9.59 \times 10^{13}$	85	2.31
455	2.99	$3.46 \times 10^{14}$	86	2.21

cence intensity of the donor in the presence of AO is shown in Figure 4c. Picosecond-resolved FRET is clearly evident from Figure 4d–f and Table 3. As is evident from Figure 4 and Tables 3 and 4, the steady-state quenching and temporal behavior of the vibronic bands distinctly follow the individual overlap integrals of the bands with the absorption of AO in the micelle. The estimated D–A distance of 2.48 nm was also found to be comparable to that of the BP–Et distance. Notably,

the diameter of the SDS micelle is around 5 nm, as reported in one of our recent works,<sup>[21]</sup> and BP is around 0.9 nm in length and 0.5 nm in width. Therefore, despite the fact that BP is in the hydrophobic core of the micelle, it remains closer to one part of the micellar surface than to the other depending on variations in the distance between BP and the probes residing on the micellar surface.

The Et and AO energy acceptors considered so far offer different degrees of spectral overlap with all of the vibronic bands of BP. The consequence of the dif-

ferent values of  $J(\lambda)$  for the vibronic bands is described above. Unambiguous evidence for the effect of different values of  $J(\lambda)$  for the vibronic bands on the corresponding FRET efficiency from the bands can be achieved in a control experiment, in which the acceptor offers essentially no overlap with some bands and partial overlap with others. The use of CV as a potential acceptor offers essentially no overlap with band 1 ( $\lambda_{em} = 410$  nm) and significant overlap with band 3 ( $\lambda_{em} = 455$  nm). The interaction of CV probe molecules with the SDS micelle was investigated previously, and it was concluded that CV resides at the surface of the micelle.<sup>[22]</sup> The overall and deconvoluted values of  $J(\lambda)$  are shown in Figure 5a,b, respectively. The overlap integral,  $J(\lambda)$ , between the deconvoluted emission spectrum of the donor and the absorption spectrum of the CV acceptor was characterized for each emission peak and is tabulated in Table 5. For a better view of the mentioned areas of overlap between the deconvoluted emission spectrum of the BP donor and the absorption spectrum of the CV acceptor, the overlapped region was magnified and is shown in the inset of Figure 5b. The steady-state fluorescence quenching of the BP donor in the presence of the CV acceptor is shown in Figure 5c. As is evident from Figure 5c, steady-state

**Table 5.** Comparison of the Förster distance ( $R_0$ ), overlap integral  $J(\lambda)$  (between the emission spectrum of the BP donor and the absorption spectrum of the CV acceptor) obtained at the three deconvoluted emission peaks of the donor along with the energy transfer efficiency ( $E$ ) and the D–A distance ( $r$ ) calculated from time-resolved experiments in the presence of the CV acceptor.

$\lambda_{em}$ (BP) [nm]	$R_0$ [nm]	$J(\lambda)$ [ $M^{-1} cm^{-1} nm^4$ ]	$E$ [%]	$r$ [nm]
410	1.03	$1.26 \times 10^{11}$	0	–
430	1.32	$6.04 \times 10^{11}$	86	0.75
455	1.66	$1.02 \times 10^{13}$	91	1.13

fluorescence quenching of BP occurs at all of the vibronic bands of BP, which can be due to the formation of nonradiative D–A complexes in the ground state or due to energy transfer, and hence, steady-state fluorescence quenching is in-

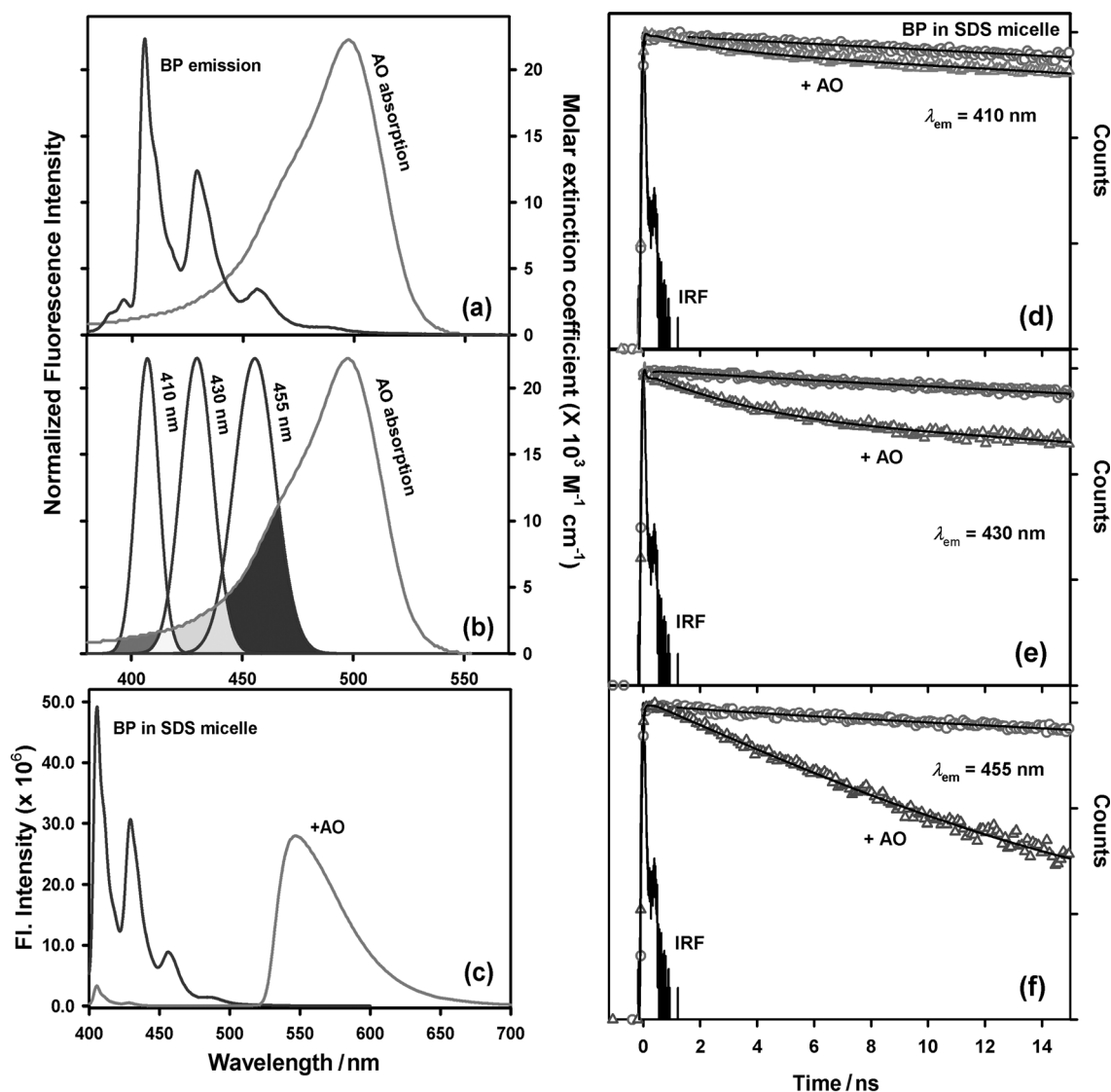


**Figure 4.** Overlap of the emission spectrum of BP with the absorption spectrum of AO in 100 mM SDS ( $\approx 1.48$  mM micellar concentration) without (a) and with (b) the deconvolution of the emission spectrum of BP at specific wavelengths of 410, 430, and 455 nm. c) The emission spectrum of BP in the SDS micelle before and after the addition of the AO acceptor. Picosecond-resolved fluorescence transients of the BP donor molecules bound to SDS micelles with ( $\Delta$ ) and without ( $\circ$ ) the AO acceptor at d) 410, e) 430, and f) 455 nm.  $\lambda_{\text{ex}} = 350$  nm for (a) and (b) and  $\lambda_{\text{ex}} = 375$  nm for (c)–(f).

conclusive, as reported earlier.<sup>[18,26]</sup> Notably, band 3 is differentially quenched than the others as a consequence of a larger value of  $J(\lambda)$  with the CV acceptor. To compare the energy-transfer efficiency of the donor from its various vibronic structures, the fluorescence transients of the donor at its different emission peaks (410, 430, and 455 nm) were monitored in the absence and in the presence of CV (Figure 6 and Table 3). The corresponding FRET parameters are tabulated in Table 5. As is evident from the inset of Figure 5b, there is negligible or almost no overlap between the emission spectrum of BP at 410 nm and the CV absorption spectrum, which consequently produces no fluorescence lifetime quenching of the BP donor at 410 nm in the presence of the CV acceptor. However, there is significant lifetime quenching of the fluorophore at the other two vibronic bands (430 and 455 nm). This observation is consistent with our previous results for which the other two

acceptors show overlap-integral-dependent fluorescence lifetime quenching of the individual vibronic bands. Furthermore, the present observation, for which we find no quenching at vibronic band 1 due to negligible overlap with the absorption spectrum of CV, highlights the conclusive evidence of differential FRET from the vibronic bands of the BP donor. Notably, our study finds that the differential behavior of the vibronic bands of BP that undergo FRET with different energy acceptors is dependent on the individual spectral overlap of the vibronic bands in a qualitative manner. To find a mathematical relation between the FRET parameters (e.g. degree of quenching/energy-transfer efficiency) and individual spectral overlap, other factors such as vibrational coupling between the different vibronic bands in the emission spectrum of BP should also be taken into account, but this needs further investigation.

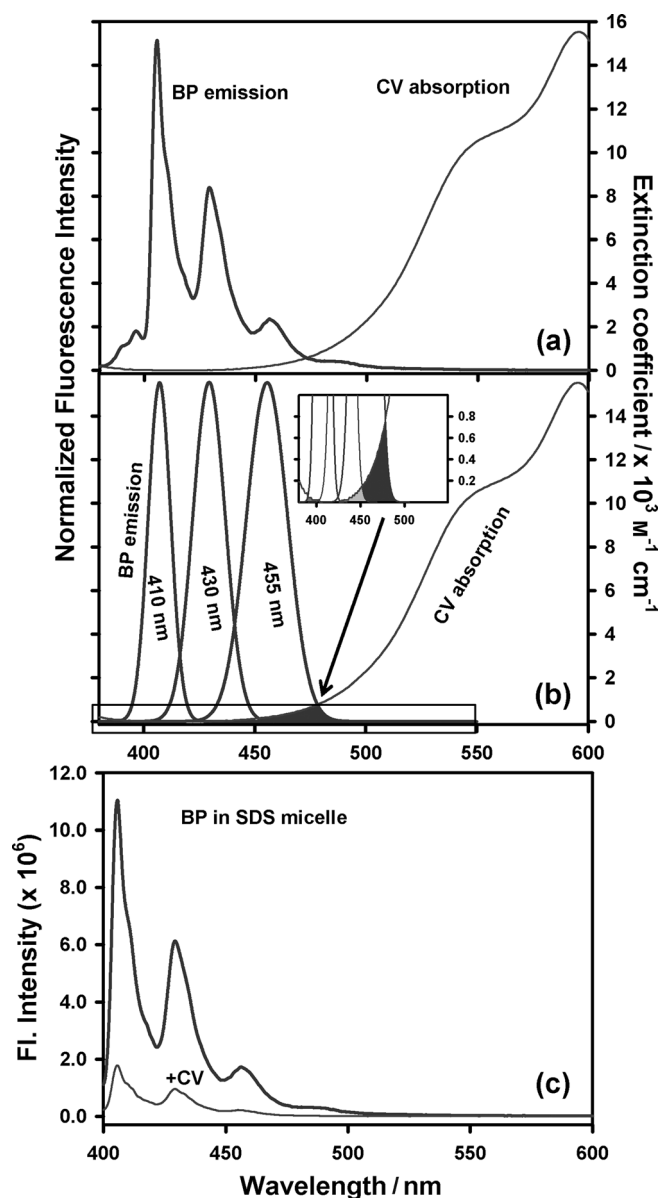


**Figure 5.** Overlap of the emission spectrum of BP with the absorption spectrum of CV in 100 mM SDS ( $\approx 1.48$  mM micellar concentration) without (a) and with (b) the deconvolution of the emission spectrum of BP at specific wavelengths of 410, 430, and 455 nm. The inset in (b) is a magnified view of the overlapped region marked by a rectangle. c) The emission spectrum of BP in the SDS micelle before and after the addition of the CV acceptor.  $\lambda_{\text{ex}} = 350$  nm for (a) and (b) and  $\lambda_{\text{ex}} = 375$  nm for (c).

### Comparison of the Differential Behavior of the Vibronic Bands of BP under FRET with that of the Different Dyes in a Dye-Blend Representing Different Electronic States

From our studies, differential FRET from various vibronic bands of BP can be compared with dye-blend (mixture of dyes) under FRET to an energy acceptor in solution. In this regard, we investigated the FRET of a mixture of three QDs having different emission maxima to the CV energy acceptor. Figure 7a,b show the overall and deconvoluted overlap between the emission spectra of the QDs (donor) and the absorption spectrum

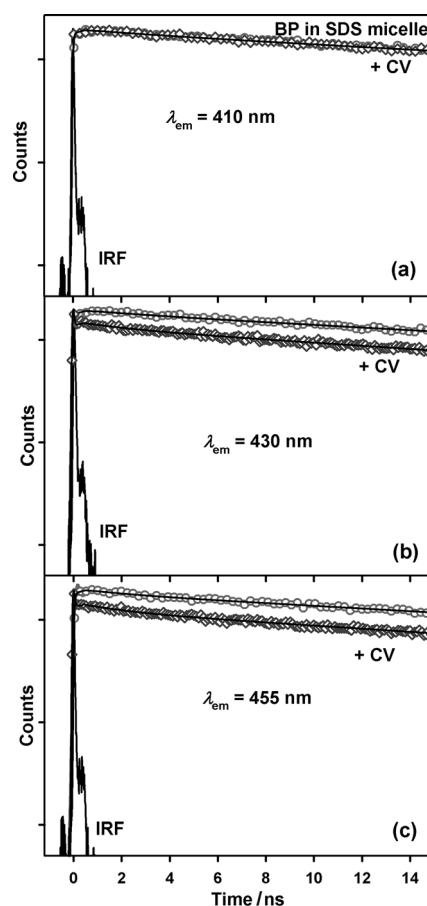


**Figure 6.** Picosecond-resolved fluorescence transients of the BP donor molecules bound to SDS micelles with ( $\diamond$ ) and without ( $\circ$ ) the CV acceptor at a) 410, b) 430, and c) 455 nm.  $\lambda_{\text{ex}} = 375$  nm.

of CV (acceptor) in toluene, respectively. The overlap integral,  $J(\lambda)$ , between the deconvoluted emission spectrum of the QDs donor and the absorption spectrum of the CV acceptor was characterized and is tabulated in Table 6. Picosecond-resolved FRET is clearly evident from Figure 7c and Table 7. The measured distance  $r$  between the QDs and CV is greater than the radii of the QDs (mentioned in the Experimental Section) in all cases, and with an increase in the diameter of the QDs, the CV acceptor gets closer to the surface of the QDs, as shown from the calculated D–A distances given in Table 6. As is evident from Figure 7 and Tables 6 and 7, the temporal behavior of the QDs in the presence of the CV acceptor in toluene is comparable to the overlap-integral-dependent quenching behavior of the individual vibronic bands of BP with different acceptors in the micelle.

### Verification of the Introduced Method of Differential FRET Calculation by Employing the Standard Theoretical Framework and D–A Distribution

The suitability of the differential procedure over integral analysis introduced in the present study in the standard theoretical framework of FRET to estimate the average number of quenchers/quenching constants developed by Infelta and Tachiya<sup>[21]</sup>

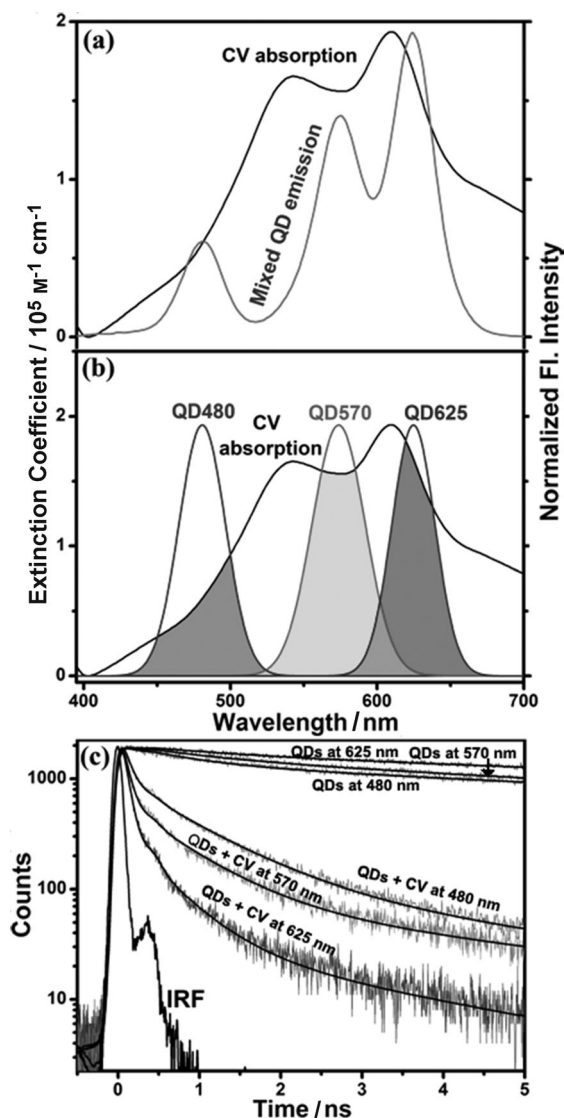


**Figure 7.** Overlap of the emission spectrum of mixed QDs (donor) with the absorption spectrum of CV (acceptor) without (a) and with (b) the deconvolution of the emission spectrum of mixed QDs at specific wavelengths of 480, 570, and 625 nm. c) Picosecond-resolved fluorescence transients of the donor (mixed QDs) in the absence and in the presence of the CV acceptor monitored at 480, 570, and 625 nm.  $\lambda_{\text{ex}} = 375 \text{ nm}$ .

was also investigated. We determined the values of the parameters  $m$ ,  $k_q$ , and  $k_0$  as described in the Experimental Section by fitting Equation (12) to the decay curves of the BP donor molecules in the absence and in the presence of the Et, AO, and CV acceptors (Figure 8a and Table 8).

Figure 8a shows the time-resolved fluorescence transients of BP monitored at its different emission peaks (410, 430, and 455 nm) in the absence and in

**Table 6.** Comparison of the Förster distance ( $R_0$ ), overlap integral  $J(\lambda)$  (between the emission spectra of the QD donors and the absorption spectrum of the CV acceptor) obtained at the three deconvoluted emission peaks of the QD donors along with the energy transfer efficiency ( $E$ ) and D–A distance ( $r$ ) calculated from time-resolved experiments in the presence of the CV acceptor.

$\lambda_{\text{em}}(\text{QDs})$ [nm]	$R_0$ [nm]	$J(\lambda)$ [ $\text{M}^{-1} \text{ cm}^{-1} \text{ nm}^4$ ]	$E$ [%]	$r$ [nm]
480	5.2	$7 \times 10^{15}$	95	3.2
570	6.0	$16.7 \times 10^{15}$	97	3.4
625	6.4	$22.5 \times 10^{15}$	99	2.9

the presence of Et, AO, and CV fitted with Equation (12). Given that our time-resolved studies (Figure 6a and Table 3) show that CV does not quench the fluorescence lifetime of the BP donor at 410 nm, the corresponding fluorescence transient was not fitted with the equation of the kinetic model [Eq. (12)]. As evidenced from Figure 8a, the model describes the decay curves reasonably well. The quenching parameters are summarized in Table 8. Upon fitting the decay curves of BP with the kinetic model mentioned above, it is apparent that the distribution of the acceptor molecules on the micellar surface does not change with the wavelength at which the donor emission is monitored.

As summarized in Table 8, the mean number of acceptor molecules associated with the micelle ( $m$ ) remains the same at 0.8, 1, and 0.7 for Et, AO, and CV, respectively, at the three wavelengths corresponding to the three emission peaks of BP. The fact that the value of  $m$  is independent of the vibronic structure of the donor provides authenticity of the analysis procedure. However, the value of the quenching rate constant ( $k_q$ ) due to the acceptors depends on the wavelength at which the donor emission is monitored; this value reaches a maximum at 455 nm and reaches a minimum at 410 nm with an intermediate value at 430 nm. The nature of the change in  $k_q$  is similar to that of the energy-transfer efficiency mentioned above, and this holds well to the fact that  $k_q$  is also proportional to the overlap integral between the emission spectrum of the donor and the absorption spectrum of the acceptor. Further studies are required to understand better the observed variation of  $k_q$  with the emission wavelength of the BP donor molecules. The total decay constant ( $k_0$ ) of the excited probe

**Table 7.** Lifetime components ( $\tau$ ) of various QDs at their characteristic emission peaks in the absence and in the presence of the CV acceptor. The mixture of QDs consists of QD480, QD570, and QD625 having emission maxima at 480, 570, and 625 nm, respectively.

Sample	$\lambda_{\text{em}}$ [nm]	$\tau_1$ [ns] (rel. contrib. [%]) <sup>[a]</sup>	$\tau_2$ [ns] (rel. contrib. [%]) <sup>[a]</sup>	$\tau_3$ [ns] (rel. contrib. [%]) <sup>[a]</sup>	$\tau_{\text{av}}$ <sup>[b]</sup> [ns]
QD	480	0.80 (36)	12.70 (64)	–	8.40
mixture	570	1.10 (25)	11.40 (75)	–	8.70
	625	1.10 (17)	16.20 (83)	–	13.60
QD	480	0.10 (72)	0.90 (24)	4.40 (4)	0.40
mixture + CV	570	0.10 (85)	0.70 (13)	4.80 (2)	0.30
	625	0.10 (93)	0.50 (6)	3.00 (1)	0.10

[a] Relative contribution of the component. [b]  $\tau_{\text{av}}$  is the average lifetime. Error  $\pm 5\%$ .

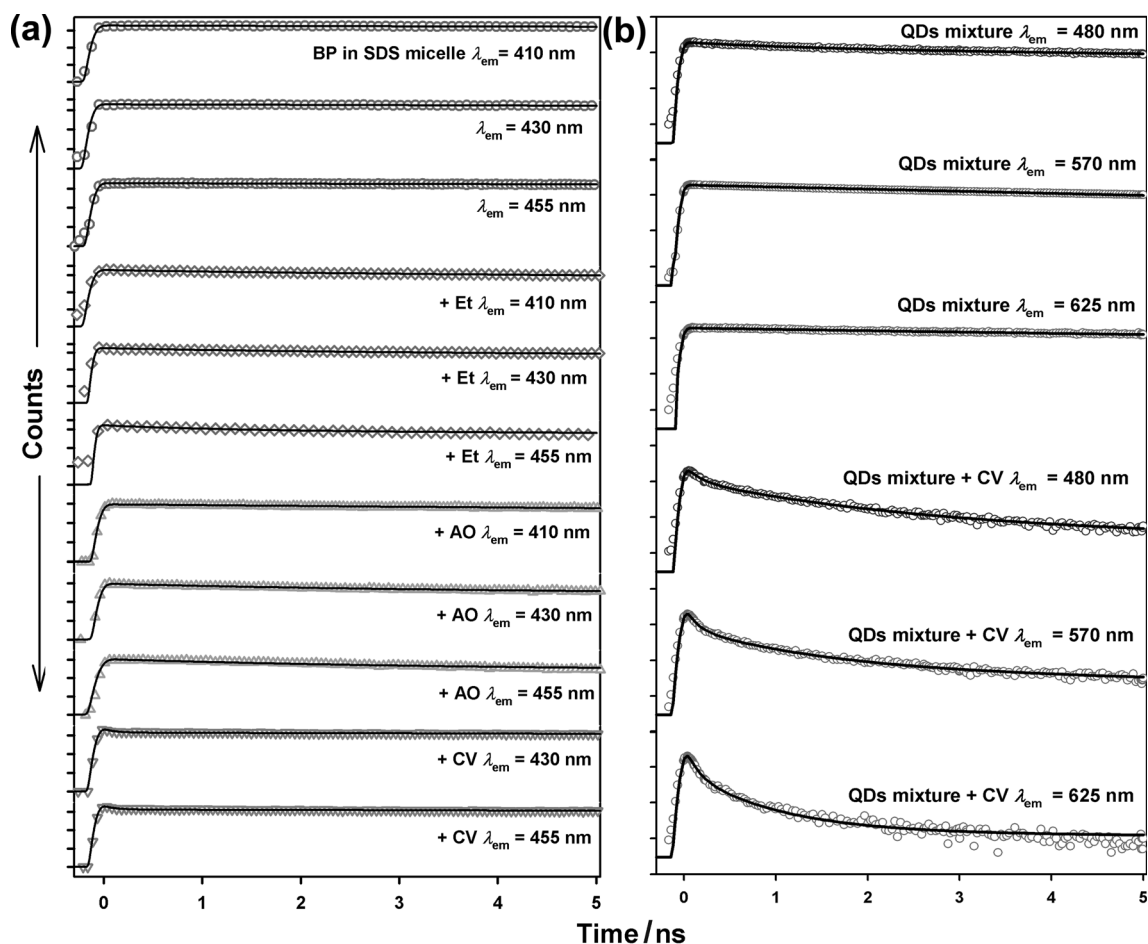


**Figure 8.** a) Fluorescence transients of the BP donor molecules bound to SDS micelles with ( $\diamond$ ,  $\triangle$ ,  $\nabla$ ) and without ( $\circ$ ) the Et, AO, and CV acceptor molecules monitored at wavelengths of 410, 430, and 455 nm. The symbols  $\diamond$ ,  $\triangle$ , and  $\nabla$  in the fluorescence transients of BP represent the presence of the Et, AO, and CV acceptors in the micelle, respectively. b) The fluorescence transients of the donor (mixed QDs) in toluene in the absence and in the presence of the CV acceptor, monitored at wavelengths of 480, 570, and 625 nm. All the transients were fitted with the kinetic model developed by Infelta and Tachiya (see text). The y axis is presented in log scale and the baselines of the transients are vertically shifted for clarity.

Sample	$\lambda_{em}$ [nm]	$K_0$ [ $ns^{-1}$ ]	$K_q$ [ $ns^{-1}$ ]	$m$
BP in SDS micelle	410	0.032	–	–
	430	0.032	–	–
	455	0.032	–	–
BP + Et in SDS micelle	410	0.032	0.24	0.8
	430	0.032	0.35	0.8
	455	0.032	0.64	0.8
BP + AO in SDS micelle	410	0.032	0.07	1
	430	0.032	0.27	1
	455	0.032	0.30	1
BP + CV in SDS micelle	430	0.032	8.97	0.7
	455	0.032	9.23	0.7

in the absence of a quencher remains the same at all of the three monitored wavelengths with a value of  $0.032 \text{ ns}^{-1}$ .

The above-mentioned kinetic model was also applied for the quenching of the QDs by the CV acceptor in toluene. We determined the values of the parameters  $m$ ,  $k_{qt}$ ,  $k_{or}$ ,  $m$ , and  $k_q$  by

fitting Equations (13) and (14) to the decay curves of the QDs in the absence and in the presence of the acceptor (as described in the Experimental Section), and they are tabulated in Table 9. The corresponding fitting curves are shown in Figure 8b.

To get an idea of the probability distribution of the D–A distance, we analyzed the time-resolved decay transients of the BP donor in the presence and in the absence of the Et acceptor as shown in Figure 9a to construct the distance distribution function,  $P(r)$  (see the Experimental Section for details). As evidenced in Figure 9b–d, the half width (hw) of the distance distribution was  $3.3 \text{ \AA}$  for all of the three vibronic bands under consideration. Similarly, the fluorescence transients of the QD480, QD570, and QD625 donors in toluene in the absence and in the presence of the CV acceptor were fitted upon considering the distance distribution between the donor and the acceptor in toluene, as shown in Figure 10a, and the hw of the distance distribution was  $3.3$ ,  $4.4$ , and  $3.3 \text{ \AA}$  for QD480, QD570, and QD625, respectively, as shown in Figure 10b–d.

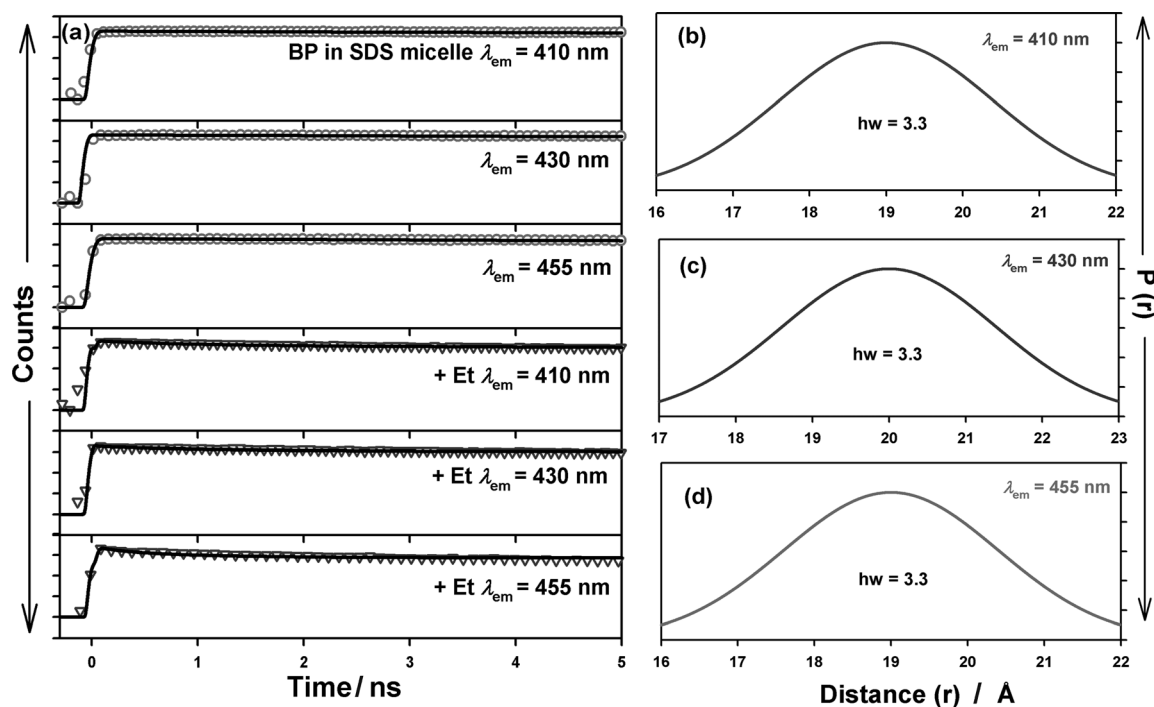


**Figure 9.** a) Fluorescence transients of BP in the SDS micelle in the absence ( $\circ$ ) and in the presence ( $\nabla$ ) of the Et acceptor as monitored at 410, 430, and 455 nm and fitted upon considering the distance distribution between the donor and acceptor in the SDS micelle. The probability of distance distribution  $P(r)$  with respect to the mean distance between the BP donor and the Et acceptor for different vibronic bands under consideration having emission maxima at b) 410, c) 430, and d) 455 nm.

**Table 9.** Overview of the quenching parameters for QDs in the absence and in the presence of the CV acceptor by using the kinetic model developed by Infelta–Tachiya.

Sample	$\lambda_{em}$ [nm]	$k_0$ [ $ns^{-1}$ ]	$m_i$	$k_{qt}$ [ $ns^{-1}$ ]	$m$	$k_q$ [ $ns^{-1}$ ]
QD mixture	480	0.07	0.41	0.67	–	–
	570	0.095	0.21	0.50	–	–
	625	0.03	1.12	0.06	–	–
QD mixture + CV	480	0.07	3.31	0.38	0.93	6.40
	570	0.095	2.86	0.62	1.43	8.46
	625	0.03	4.03	0.99	1.56	8.20

Finally, we showed that differential  $J(\lambda)$  analysis is equally acceptable to the standard theoretical framework for further interpretation of FRET data including the Infelta–Tachiya model and  $P(r)$  analysis techniques. Our reported studies may find importance in FRET analysis of the biologically relevant pyrene class of molecules.

### 3. Conclusions

We have investigated the effect of the excited-state lifetime of the well-known biological probe and food carcinogen benzo[*a*]pyrene (BP) in various solvents with different polarity/proticity/dielectric constants and polarizabilities. Although the steady-state spectral shift was expected to follow theoretical models, time-resolved studies of a number of solvents clearly invite better theoretical understanding of the photophysics of BP. Our present study also highlights the importance of considering the differential spectral overlap of the vibronic bands of BP undergoing FRET as a consequence of dipole–dipole interaction with an organic molecule in a confined environment. The differential behavior of the vibronic bands of BP under FRET was compared with the behavior of a dye molecule in a dye-blend under FRET, and reasonable similarity was found.

### Experimental Section

#### Sample Preparation

Benzo[*a*]pyrene (BP), ethidium (Et) bromide salt, acridine orange (AO), crystal violet (CV), and toluene were obtained from Sigma. Three quantum dots (QDs), namely, Lake Placid Blue (LPB, crystal diameter 1.9 nm; QD480), Birch yellow (Bir-yellow, crystal diameter 3.2 nm; QD570), and Maple red-orange (Map-red, crystal diameter 5.2 nm; QD625) having emission maxima in toluene at 480, 570, and 625 nm, respectively, were purchased from Evident Technology, USA. Dioxane, dimethyl sulfoxide (DMSO), diethyl ether, heptane, dimethyl formamide (DMF), and acetonitrile were obtained from Spectrochem, whereas ethanol, methanol, ethylene glycol, acetone, and benzene were obtained from Merck. Cyclohexane was obtained from SRL, and sodium dodecyl sulfate (SDS) was acquired from Fisher Scientific and used without further purification. The concentration of BP was kept very low ( $\approx 5 \mu M$ ) to avoid the

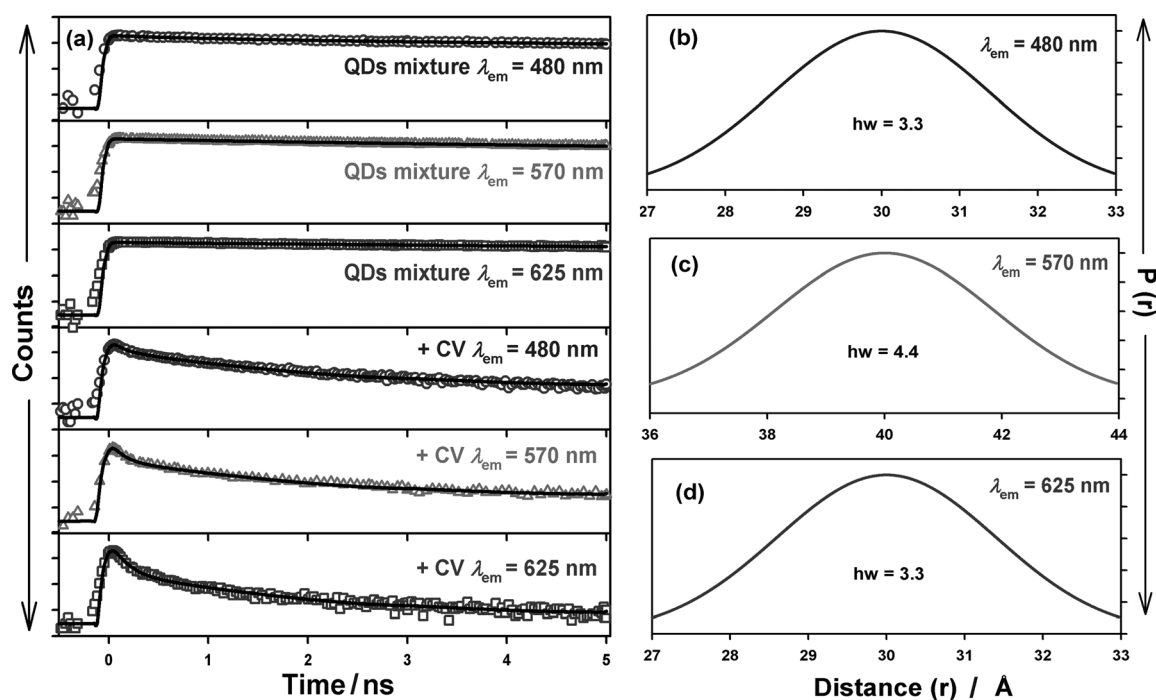


**Figure 10.** a) Fluorescence transients of the QD mixture (QD480, QD570, and QD625) in toluene in the absence and in the presence of the CV acceptor and fitted upon considering the distance distribution between the donor and the acceptor in toluene. The probability of the distance distribution [ $P(r)$ ] with respect to the mean distance between the b) QD480 c) QD570, and d) QD625 donors and the CV acceptor in toluene.

formation of aggregates while monitoring its fluorescence transients in different solvents. SDS solutions were prepared in doubly distilled water. The concentration of SDS used was 100 mM, that is, the micellar concentration was estimated to be 1.48 mM, whereas the quencher concentrations were maintained at 0.80, 0.35, and 0.12 mM for Et, AO, and CV, respectively. In all of the experiments, the concentrations of the micelles were much higher than those of the acceptors to ensure that no more than one acceptor was held by one micelle. To prevent homomolecular energy transfer between the donor molecules and to ensure efficient energy transfer between the donor and acceptor in the micellar solution, the concentration of the BP donor molecules was kept low (1.2  $\mu\text{M}$ ). Furthermore, in the micellar solution the [donor]/[micelle] ratio was  $8 \times 10^{-4}$  ([donor]/[micelle] = 1.2/1480), which avoided the existence of multiple donors in the same micelle. The low optical density of the samples at the excitation wavelengths (350 and 375 nm) circumvents the possibility of inner filter effects.

### Steady-State and Time-Resolved Studies

Steady-state absorption and emission spectra were measured with a Shimadzu Model UV-2450 spectrophotometer and Jobin-Yvon Model Fluoromax-3 fluorimeter, respectively. All picosecond transients were measured by using a commercially available (Edinburgh Instrument, UK) picosecond-resolved time-correlated single photon counting (TCSPC) setup (instrument response function, IRF of 80 ps) by using a 375 nm excitation laser source (from Picoquant, Germany). Fluorescence from the sample was detected by a photomultiplier after dispersing through a double grating monochromator. For all transients, the polarizer in the emission side was adjusted to be at an angle of  $54.7^\circ$  (magic angle) with respect to the polarization axis of the excitation beam. To obtain a reasonably good signal-to-noise ratio, all the TCSPC experiments were performed with at least 5000 counts. The femtosecond-resolved fluorescence

was measured by using a femtosecond upconversion setup (FOG 100, CDP); the sample was excited at 375 nm (0.5 nJ per pulse) by using the second harmonic of a mode-locked Ti-sapphire laser with an 80 MHz repetition rate (Tsunami, Spectra Physics), pumped by 10 W Millennia (Spectra Physics). The fundamental beam was frequency doubled in a nonlinear crystal (1 mm BBO,  $\theta = 25^\circ$ ,  $\varphi = 90^\circ$ ). The fluorescence emitted from the sample was up-converted in a nonlinear crystal (0.5 mm BBO,  $\theta = 10^\circ$ ,  $\varphi = 90^\circ$ ) by using a gate pulse of the fundamental beam. The upconverted light was dispersed in a double monochromator and detected by using photon counting electronics. A cross-correlation function obtained by using the Raman scattering from water displayed a full width at half maximum (FWHM) of 165 fs.

### Förster Resonance Energy Transfer (FRET)

To estimate the FRET efficiency of the BP donor to the different acceptors (i.e. Et, AO, and CV) and hence to determine distances ( $r$ ) of the D–A pairs, we followed the methodology described in Chapter 13 of ref. [26]. The Förster distance ( $R_0$ ) is given by Equation (1):

$$\frac{R_0}{\text{\AA}} = 0.211 [\kappa^2 n^{-4} Q_D J(\lambda)]^{1/6} \quad (1)$$

in which  $\kappa^2$  is a factor describing the relative orientation in space of the transition dipoles of the donor and the acceptor. The value of  $\kappa^2$  is calculated from Equation (2):

$$\kappa^2 = (\cos \theta_T - 3 \cos \theta_D \times \cos \theta_A)^2 \quad (2)$$

in which  $\theta_T$  is the angle between the emission transition dipole of the donor and the absorption transition dipole of the acceptor and  $\theta_D$  and  $\theta_A$  are the angles between these dipoles and the vector joining the donor and the acceptor.<sup>[26]</sup> In the micellar system, the

donor and acceptor molecules can be bound simultaneously without any restriction on the relative orientation of their transition dipole moments. Thus, the orientation parameter ( $\kappa^2$ ) can be taken as 0.667.<sup>[26]</sup> Moreover, as the sixth root is taken to calculate the distance, variation of  $\kappa^2$  from the value for random orientation ( $\kappa^2 = 2/3$ ) to that for parallel dipolar orientation ( $\kappa^2 = 1$ ), or to that for head-to-tail parallel transition dipoles ( $\kappa^2 = 4$ ), the calculated distance can be in error by no more than 35%.<sup>[26]</sup> The refractive index,  $n$ , of the medium was measured as 1.3, which is apparent, because the space separating the donor and the acceptor consists of the hydrophobic tails (alkyl chain) of the SDS micelle and the refractive index of similar alkanes such as pentane, hexane, heptane, dodecane, and so on varies between 1.30 and 1.42. The quantum yield,  $Q_D$ , of the donor in the absence of the acceptor was calculated according to Equation (3):<sup>[32]</sup>

$$Q = Q_R \left( \frac{I}{I_R} \right) \left( \frac{OD_R}{OD} \right) \left( \frac{n^2}{n_R^2} \right) \quad (3)$$

in which  $Q$  is the quantum yield of BP in the SDS micelle and  $Q_R$  is the quantum yield of the reference (Hoechst 33258 in SDS),  $I$  and  $I_R$  are the integrated fluorescence intensities of BP and the reference, respectively,  $OD$  and  $OD_R$  are the optical densities of BP and the reference at the excitation wavelength, respectively, and  $n$  and  $n_R$  are the refractive indices of BP and the reference solutions, respectively. The absolute quantum yield of Hoechst 33258<sup>[14]</sup> in SDS was taken to be 0.54. Refractive indices of the solutions were measured by using a Rudolph J357 automatic refractometer. The quantum yield of BP in the SDS micelle was near unity, and the relative value of  $Q_D$  of BP in the SDS micelle at the different emission peaks was calculated upon deconvoluting the BP emission spectrum at its emission peaks around 410, 430, and 455 nm and was calculated to be 0.45, 0.43, and 0.10, respectively.

The overlap integral,  $J(\lambda)$ , which expresses the degree of overlap between the emission spectrum of the donor and the absorption spectrum of the acceptor is given by Equation (4):

$$J(\lambda) = \frac{\int_0^\infty F_D(\lambda) \varepsilon(\lambda) \lambda^4 d(\lambda)}{\int_0^\infty F_D(\lambda) d(\lambda)} \quad (4)$$

in which  $F_D(\lambda)$  is the fluorescence intensity of the donor in the wavelength range from  $\lambda$  to  $\lambda + d\lambda$ , and this value is dimensionless;  $\varepsilon(\lambda)$  is the extinction coefficient (in  $\text{m}^{-1} \text{cm}^{-1}$ ) of the acceptor at  $\lambda$ . If  $\lambda$  is in nm, then  $J(\lambda)$  is in units of  $\text{m}^{-1} \text{cm}^{-1} \text{nm}^{-4}$ . Once the value of  $R_0$  is known, the D–A distance ( $r$ ) can be calculated by using Equation (5):

$$r^6 = [R_0^6 (1 - E)]/E \quad (5)$$

in which  $E$  is the efficiency of the energy transfer, which is calculated from the average lifetimes of the donor in the absence and in the presence of acceptors [ $\tau_D$  and  $\tau_{DA}$ , Eq. (6)]:

$$E = 1 - \frac{\tau_{DA}}{\tau_D} \quad (6)$$

### Infelta–Tachiya Model (Kinetic Model)

The decay of an excited BP probe in a micelle may be described by the following kinetic model [Eqs. (7) and (8)]:<sup>[21]</sup>



in which  $P_n^*$  and  $P_n$  stand for a micelle containing  $n$  quencher molecules with and without an excited probe, respectively,  $k_0$  is the total decay constant of the excited state in the absence of a quencher, and  $k_q$  is the rate constant for quenching of an excited probe in a micelle containing one quencher molecule. In this kinetic model, it is assumed that the distribution of the number of quenchers attached to one micelle follows a Poisson distribution,<sup>[33]</sup> namely [Eq. (9)],

$$p(n) = (m^n/n!) \exp(-m) \quad (9)$$

in which  $m$  is the mean number of quenchers in a micelle [Eq. (10)]:

$$m = k_+[A]/k_- \quad (10)$$

in which  $k_+$  is the rate constant for entry of a quencher molecule into a micelle,  $k_-$  is the rate constant for exit of a quencher molecule from a micelle containing one quencher molecule, and  $A$  is the quencher molecule in the aqueous phase. On the basis of the above model, the equation for the total concentration  $P^*(t)$  of excited probes at time  $t$  is given by Equation (11):<sup>[21]</sup>

$$P^*(t) = P^*(0) \exp \left[ - \left( k_0 + \frac{k_0 k_+ [A]}{k_- + k_q} \right) t \right] - \frac{k_q^2 k_+ [A]}{k_- (k_- + k_q)^2} \{ 1 - \exp [ - (k_- + k_q) t ] \} \quad (11)$$

If  $k_-$  is much smaller than  $k_q$ , then this equation reduces to Equation (12):

$$P^*(t) = P^*(0) \exp \{ -k_0 t - m [1 - \exp(-k_q t)] \} \quad (12)$$

The observed fluorescence transients were fitted by using a nonlinear least-squares fitting procedure (software SCIENTIST) to a function ( $X(t) = \int_0^t E(t') P(t-t') dt'$ ) comprising the convolution of the instrument response function [IRF,  $E(t)$ ] with exponential ( $P^*(t) = P^*(0) \exp \{ -k_0 t - m [1 - \exp(-k_q t)] \}$ ). The purpose of this fitting was to obtain the decays in an analytic form suitable for further data analysis.

For the QDs, along with the CV acceptor, some unidentified traps exist that further cause quenching of the lifetime of the excited QD probe, which are also taken into account. If the distribution of the number of unidentified traps around the QDs donor follows a Poisson distribution with the average number ( $m_t$ ), the decay curves of the excited state of the QDs in toluene in the absence and in the presence of CV are described by [Eqs. (13) and (14)]:<sup>[34]</sup>

$$P^*(t, 0) = P^*(0) \exp \{ -k_0 t - m_t [1 - \exp(-k_{qt} t)] \} \quad (13)$$

$$P^*(t, m) = P^*(0) \exp \{ -k_0 t - m_t [1 - \exp(-k_{qt} t)] \} - m [1 - \exp(-k_q t)] \quad (14)$$

in which the quenching rate constant ( $k_{qt}$ ) by unidentified traps may be different from that ( $k_q$ ) by the CV acceptor.

## Distance Distribution in Donor–Acceptor Systems

The distance distribution between the donor and acceptor was estimated according to the procedure described in the literature.<sup>[26,35]</sup> The observed fluorescence transients of the BP donor molecules in the absence of the Et acceptor in the micelle were fitted by using a nonlinear least-squares fitting procedure (software SCIENTIST) to the following function [Eq. (15)]:

$$I_D(t) = \int_0^t E(t')P(t' - t)dt' \quad (15)$$

which comprises the convolution of the instrument response function [IRF,  $E(t)$ ] with the exponential ( $P(t) = \sum_i \alpha_{Di} \exp(-t/\tau_{Di})$ ). The convolution of the distance distribution function  $P(r)$  in the fluorescence transients of the donor in the presence of the acceptor in the system under study (i.e. micelle) was estimated by using the same software (SCIENTIST) in the following way.

The intensity decay of the D–A pair, spaced at a distance  $r$ , is given by Equation (16):

$$I_{DA}(r, t) = \sum_i \alpha_{Di} \exp \left[ -\frac{t}{\tau_{Di}} - \frac{t}{\tau_{Di}} \left( \frac{R_0}{r} \right)^6 \right] \quad (16)$$

and the intensity decay of the sample considering  $P(r)$  is given by Equation (17):

$$I_D(t) = \int_{r=0}^{\infty} P(r)I_{DA}(r, t)dr \quad (17)$$

in which  $P(r)$  consists of the following terms [Eq. (18)]:

$$P(r) = \frac{1}{\sigma\sqrt{2\pi}} \exp \left[ -\frac{1}{2} \left( \frac{\bar{r} - r}{\sigma} \right)^2 \right] \quad (18)$$

In this equation,  $\bar{r}$  is the mean of the Gaussian with a standard deviation of  $\sigma$ . Usually, distance distributions are described by the full width at half maxima. This half width is given by  $hw = 2.354 \sigma$ . A similar procedure was followed to find the distance distribution of the QDs donor and the CV acceptor in toluene.

## Acknowledgements

S.B. thanks the University Grant Commission (UGC), India, and N.G. thanks the Council of Scientific and Industrial Research (CSIR), India, for Research Fellowships. The authors thank Prof. M. Tachiya, National Institute of Advanced Industrial Science and Technology (AIST), Japan, for helping to develop this kinetic model. We thank the Department of Science and Technology (DST), India, for a financial grant (DST/TM/SERI/2k11/103 and SB/SI/PC-011/2013).

**Keywords:** FRET · micelles · quantum dots · ultrafast spectroscopy · vibronic fine structures

- [1] M. Graetzel, J. K. Thomas, *J. Am. Chem. Soc.* **1973**, *95*, 6885–6889.
- [2] K. Kalyanasundaram, J. K. Thomas, *J. Am. Chem. Soc.* **1977**, *99*, 2039–2044.
- [3] J. D. Morrisett, H. J. Pownall, R. T. Plumlee, L. C. Smith, Z. E. Zehner, M. Esfahani, S. J. Wakil, *J. Biol. Chem.* **1975**, *250*, 6969–6976.
- [4] J. Aguilera-Sigalat, J. Sanchez-SanMartin, C. E. Agudelo-Morales, E. Zaballos, R. E. Galian, J. Pérez-Prieto, *ChemPhysChem* **2012**, *13*, 835–844.
- [5] T. Shyamala, S. Sankaraman, A. K. Mishra, *Chem. Phys.* **2006**, *330*, 469–477.
- [6] S. C. Beck, D. T. Cramb, *J. Phys. Chem. B* **2000**, *104*, 2767–2774.
- [7] M. R. Vigil, J. Bravo, T. D. Z. Atvars, J. Baselga, *Macromolecules* **1997**, *30*, 4871–4876.
- [8] G. W. Hsu, X. Huang, N. P. Luneva, N. E. Geacintov, L. S. Beese, *J. Biol. Chem.* **2005**, *280*, 3764–3770.
- [9] K. Dutta, D. Ghosh, A. Nazmi, K. L. Kumawat, A. Basu, *PLoS One* **2010**, *5*, 1–14.
- [10] T. Kometania, I. Yoshinob, N. Miuraa, H. Okazakia, T. Ohbaa, T. Takenakaa, F. Shojia, T. Yanoa, Y. Maeharaa, *Cancer Lett.* **2009**, *278*, 27–33.
- [11] B. Schuler, E. A. Lipman, P. J. Steinbach, M. Kumke, W. A. Eaton, *Proc. Natl. Acad. Sci. USA* **2005**, *102*, 2754–2759.
- [12] A. K. Shaw, R. Sarkar, S. K. Pal, *Chem. Phys. Lett.* **2005**, *408*, 366–370.
- [13] A. R. Clapp, I. L. Medintz, H. Mattoussi, *ChemPhysChem* **2006**, *7*, 47–57.
- [14] D. Banerjee, S. K. Pal, *J. Phys. Chem. B* **2007**, *111*, 5047–5052.
- [15] F. M. Chen, *Nucleic Acids Res.* **1983**, *11*, 7231–7250.
- [16] M. Masuko, S. Ohuchi, K. Sode, H. Ohtani, A. Shimadzu, *Nucl. Acids Res.* **2000**, *28*, e34–00.
- [17] A. Kupstat, D. Knopp, R. Niessner, M. U. Kumke, *J. Phys. Chem. B* **2010**, *114*, 1666–1673.
- [18] P. Majumder, R. Sarkar, A. K. Shaw, A. Chakraborty, S. K. Pal, *J. Colloid Interface Sci.* **2005**, *290*, 462–474.
- [19] H. R. Mahler, P. S. Perlman, *Arch. Biochem. Biophys.* **1972**, *148*, 115–129.
- [20] S. K. Pal, D. Mandal, K. Bhattacharyya, *J. Phys. Chem. B* **1998**, *102*, 11017–11023.
- [21] S. Banerjee, M. Tachiya, S. K. Pal, *J. Phys. Chem. B* **2012**, *116*, 7841–7848.
- [22] G. Revillod, I. R. Antoine, E. Benichou, C. Jonin, P. F. Brevet, *J. Phys. Chem. B* **2005**, *109*, 5383–5387.
- [23] P. R. Ogilby, *Acc. Chem. Res.* **1999**, *32*, 512–519.
- [24] D. T. Cramb, S. C. Beck, *J. Photochem. Photobiol. A* **2000**, *134*, 87–95.
- [25] J. Spanget-Larsen, J. Waluk, S. Eriksson, E. W. Thulstrup, *J. Am. Chem. Soc.* **1992**, *114*, 1942–1949.
- [26] J. R. Lakowicz, *Principles of Fluorescence Spectroscopy*, Kluwer Academic/Plenum, New York, **1999**.
- [27] N. P. Gritsan, E. A. Pritchina, I. I. Barabanov, G. T. Burdzinski, M. S. Platz, *J. Phys. Chem. C* **2009**, *113*, 11579–11589.
- [28] S. Banerjee, S. Sarkar, K. Lakshman, J. Dutta, S. K. Pal, *J. Phys. Chem. B* **2013**, *117*, 3726–3737.
- [29] A. K. Shaw, S. K. Pal, *J. Phys. Chem. B* **2007**, *111*, 4189–4199.
- [30] J. W. Park, H. Chung, *Bull. Korean Chem. Soc.* **1986**, *7*, 113–116.
- [31] A. M. Wiosetek-Reske, S. Wysocki, *Spectrochim. Acta Part A* **2006**, *64*, 1118–1124.
- [32] N. Goswami, A. Makhal, S. K. Pal, *J. Phys. Chem. B* **2010**, *114*, 15236–15243.
- [33] M. Tachiya, *Chem. Phys. Lett.* **1975**, *33*, 289–292.
- [34] S. Sadhu, M. Tachiya, A. Patra, *J. Phys. Chem. C* **2009**, *113*, 19488–19492.
- [35] S. Batabyal, T. Mondol, S. K. Pal, *Biochimie* **2013**, *95*, 1127–1135.

Received: June 16, 2013

Published online on August 26, 2013